Interpretive crystal-field parameters: Application to Nd^{3+} in $GdVO_4$ and YVO_4

F. G. Anderson
Department of Physics, University of Vermont, Burlington, Vermont 05405

P. L. Summers, H. Weidner, P. Hong, and R. E. Peale
Department of Physics, University of Central Florida, Orlando, Florida 32816
(Received 6 May 1994)

A detailed spectroscopic study with crystal-field analysis of the doped laser crystal Nd:$GdVO_4$ is presented. The crystal field is expanded in terms of operators transforming as the irreducible representation of the T_d group. This allows us to interpret the crystal-field parameters in terms of a simple point-ion model. A similar analysis of Nd:YVO_4 is also made for comparison.

INTRODUCTION

The crystal $GdVO_4$ (GVO) doped with Nd^{3+} ions has recently been shown to compete favorably with Nd:YVO_4 (Nd:YVO) as the medium of choice for diode-pumped microchip lasers.[1,2] Interest in GVO arises because of its potential to be grown more easily and economically than YVO, and because its larger lattice constants reduce Nd-Nd interactions and increase the segregation coefficient closer to unity.[2] Though Nd:GVO is now commercially available,[3] a detailed spectroscopic study with crystal-field analysis has yet to be performed.

Our first purpose here is to report accurate Nd^{3+} levels and a crystal-field calculation for both GVO and YVO. This permits a quantitative discussion of the small but measurable differences in the two crystals. A second perhaps more far-reaching purpose is to present an application of our cubic parametrization for the crystal field.[4–6] The fitting parameters obtained for GVO/YVO demonstrate again the enhanced interpretational value of this parametrization over the traditional parametrization in terms of spherical harmonics.

EXPERIMENT

Samples of GVO used here were cut from single-crystal boules grown by the top-seeded solution growth method (modified Czochralski technique).[7] The nominal Nd^{3+} concentrations of the samples were 0.58 and 0.65 at. %. Spectra for these two concentrations were essentially identical. A 3-mm-thick sample of 1% Nd:YVO from a commercial laser rod was studied for comparison.

A Bomem DA8 Fourier-transform spectrometer collected both absorption and photoluminescence data, the latter being excited by a multiline Ar laser. A variety of resources were used with the spectrometer. The beamsplitter was either quartz or Ge-coated KBr; the detector, InSb operating at 77 K or a room-temperature Si photodiode. The frequency accuracy of the instrument is 0.004 cm^{-1} at 2000 cm^{-1}. A resolution of 1 cm^{-1} was sufficient to resolve all lines. Peak positions were determined interactively using a high-resolution graphics monitor and the uncertainty in the values is less than 0.5 cm^{-1} in most cases. The entire light path is in vacuum, so positions of absorption and luminescence peaks are in vacuum wave numbers. Spectra were collected at 80-K sample temperatures using a home-built liquid-nitrogen cold-finger cryostat. Data for GVO at 2 K were collected using a Janis supervaritemp liquid-helium cryostat.

Figure 1 compares the $^4I_{9/2} \rightarrow {}^4I_{11/2}$ transitions for Nd^{3+} in YVO and GVO at 80 K. The decrease in baseline at low frequency is caused by absorption from a thin layer of water ice on the sample surface. The similarity in the frequency position and relative strength of lines in

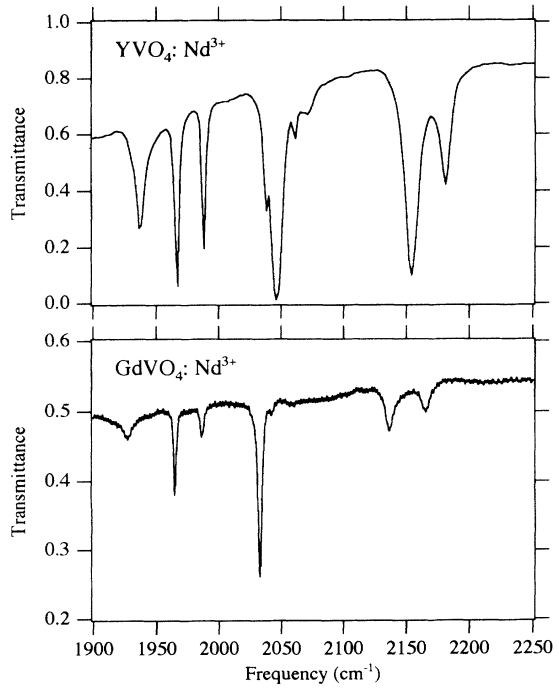

FIG. 1. $^4I_{9/2} \rightarrow {}^4I_{11/2}$ transmittance spectra for Nd^{3+} in YVO_4 and $GdVO_4$ at 80 K.

the two spectra is apparent even though the strongest YVO line is 100% deep.

Figure 2 compares the $^4I_{9/2} \rightarrow {}^4I_{13/2}$ spectra for the two materials at 80 K. Several of the YVO lines are 100% deep. Figure 3 compares the $^4I_{9/2} \rightarrow {}^4I_{15/2}$ transmission spectra. In both figures, the spectral similarity of the two crystals is clear.

In Fig. 4, a comparison is made for the $^4I_{9/2} \rightarrow {}^4F_{3/2}$ transitions at 80-K sample temperatures. Here some noticeable differences appear. For YVO the two 100% deep lines are the transitions from the ground level. The two sharp shoulders observed on their low-frequency sides arise from a second site.[8] The remaining strong lines in the spectrum are thermal replicas of the main lines, i.e., they originate from thermally populated excited levels within the $^4I_{9/2}$ manifold. For GVO, there are fewer lines. The weak line in the center of the spectrum is a thermal replica that disappears at 2 K. The deep line is asymmetric and in fact is composed of two strongly overlapping transitions. The two $^4F_{3/2}$ levels are evidently nearly degenerate in GVO. Therefore, the similarities in the GVO/YVO emission spectra will be less obvious than for their absorption spectra, since all the emission transitions we present originate in the $^4F_{3/2}$ manifold.

Figures 5–8 present the $^4F_{3/2} \rightarrow {}^4I_{15/2}$, $^4I_{13/2}$, $^4I_{11/2}$ and $^4I_{9/2}$ photoluminescence bands, respectively. In Fig. 5, both spectra were collected at 80-K sample temperatures. In Figs. 6–8, the GVO spectra were collected at 2 K to reduce as much as possible the contribution from the upper $^4F_{3/2}$ level, which is only about 3 cm^{-1} above the lower level. This contribution is already significant at 6 K. It is strong and merged with the main transitions at 80 K. Some of the weak additional lines for both materials are due to emission from a second site. Occupation of the second site is much larger in more heavily doped GVO samples, which we have studied separately.

From the photoluminescence and absorption lines, we obtain Stark levels for the $^4I\,J$ multiplets and the $^4F_{3/2}$ multiplet of Nd^{3+} in GVO. Many absorption transitions

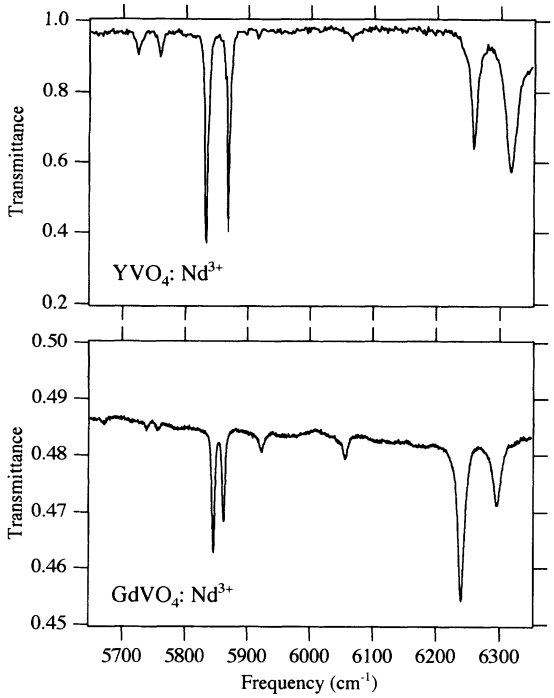

FIG. 3. $^4I_{9/2} \rightarrow {}^4I_{15/2}$ transmittance spectra for Nd^{3+} in YVO_4 and $GdVO_4$ at 80 K.

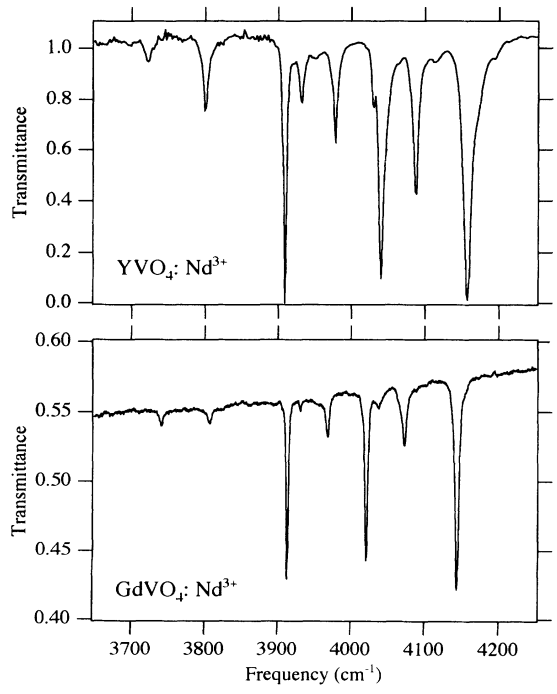

FIG. 2. $^4I_{9/2} \rightarrow {}^4I_{13/2}$ transmittance spectra for Nd^{3+} in YVO_4 and $GdVO_4$ at 80 K.

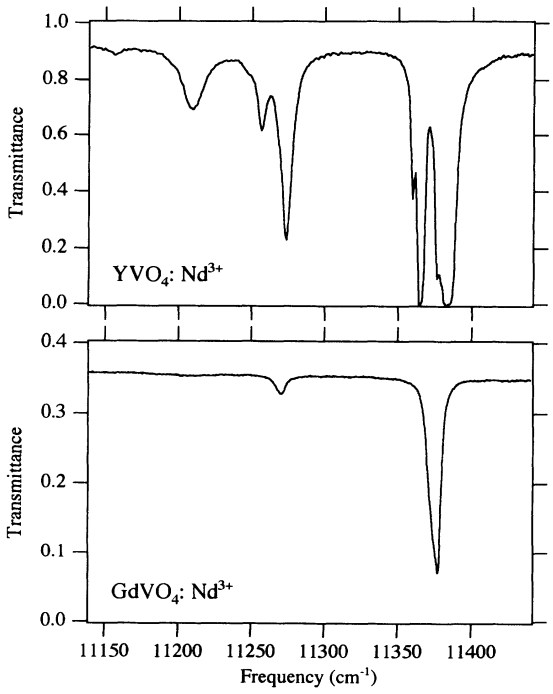

FIG. 4. $^4I_{9/2} \rightarrow {}^4F_{3/2}$ transmittance spectra for Nd^{3+} in YVO_4 and $GdVO_4$ at 80 K.

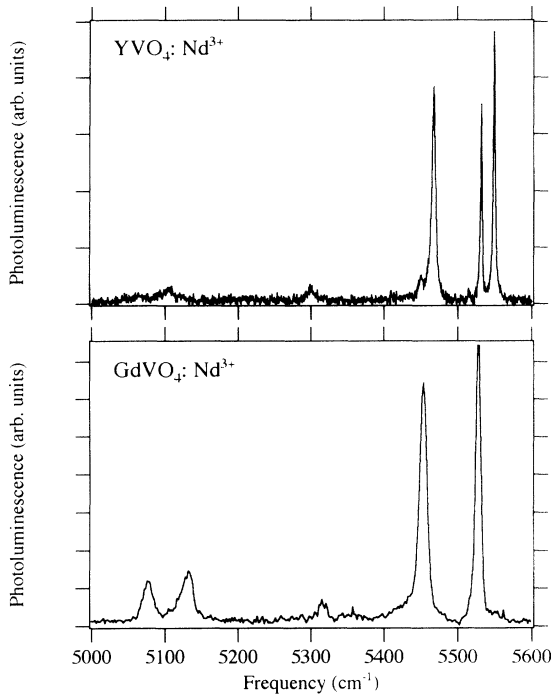

FIG. 5. $^4F_{3/2} \rightarrow {}^4I_{15/2}$ photoluminescence spectra for Nd^{3+} in YVO_4 and $GdVO_4$ at 80 K.

originating in the first two levels of $^4I_{9/2}$, which are thermally populated at 80 K, were observed and used in the analysis. A rather large Stokes shift between absorption and emission values from 2 to 4 cm^{-1} was found. Where both emission and absorption values could be used, they were averaged. Hence the GVO levels

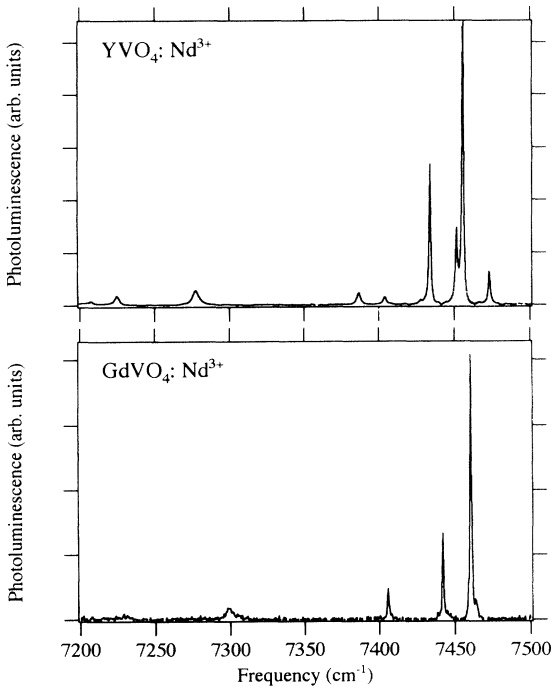

FIG. 6. $^4F_{3/2} \rightarrow {}^4I_{13/2}$ photoluminescence spectra for Nd^{3+} in YVO_4 at 80 K and $GdVO_4$ at 2 K.

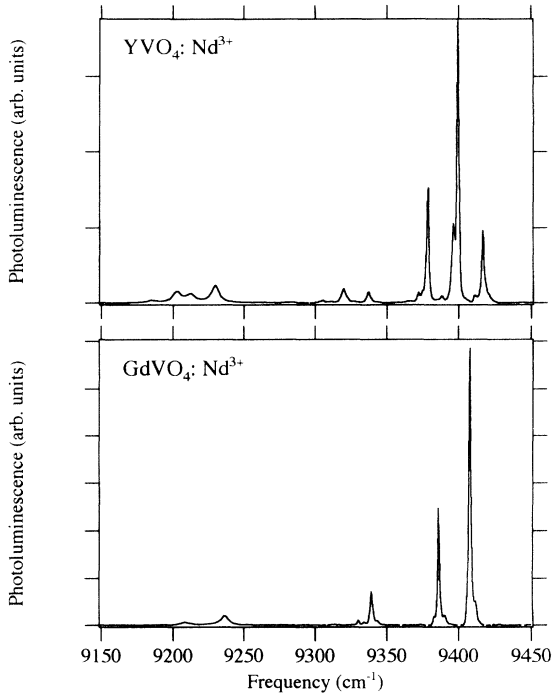

FIG. 7. $^4F_{3/2} \rightarrow {}^4I_{11/2}$ photoluminescence spectra for Nd^{3+} in YVO_4 at 80 K and $GdVO_4$ at 2 K.

TABLE I. Stark levels (cm^{-1}) of the $^4I\,J$ multiplets for Nd^{3+} in $GdVO_4$.

J multiplet	Experimental	Calculated
$^4I_{9/2}$	0.0	0.0
	103.3	102.7
	165.4	164.8
	188.0	190.4
	404.8	414.7
$^4I_{11/2}$	1 961.3	1960.5
	1 983.2	1982.2
	2 029.9	2028.2
	2 039.0	2036.5
	2 132.7	2136.1
	2 160.7	2159.5
$^4I_{13/2}$	3 909.5	3908.1
	3 928.1	3930.4
	3 964.5	3963.3
	4 020.6	4019.5
	4 070.2	4071.5
	4 141.5	4140.8
		4140.9
$^4I_{15/2}$	5 845.5	5847.2
	5 864.1	5869.1
	5 922.6	5924.9
	6 055.8	6049.4
		6139.9
	6 239.5	6235.2
		6237.3
	6 294.8	6291.8
$^4F_{3/2}$	11 369	
	11 372	

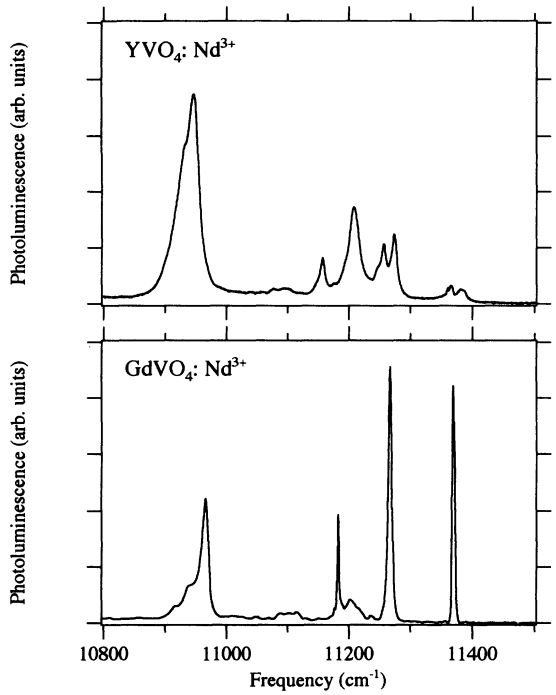

FIG. 8. $^4F_{3/2} \rightarrow {}^4I_{9/2}$ photoluminescence spectra for Nd^{3+} in YVO_4 at 80 K and $GdVO_4$ at 2 K.

presented in Table I are uncertain to within 2–4 cm^{-1}. For comparison, our determination of the Nd^{3+}:YVO levels are presented in Table II. The levels are very similar in the two crystals.

CRYSTAL-FIELD MODEL

In this section, we develop a crystal-field model for the electronic structure of the Nd^{3+} ion substituting for Gd^{3+} in GVO or for Y^{3+} in YVO. The 3+ charge state of Nd has a f^3 configuration. In accordance with Hund's rules, the ground term is ^4I; and we focus our attention on this term. As is well known, the spin-orbit interaction is rather strong within the rare-earth metals, and dominates over the crystal-field interaction. The spin-orbit interaction splits the ^4I term into manifolds of $J=\frac{9}{2}$ (the ground state), $\frac{11}{2}$, $\frac{13}{2}$, and $\frac{15}{2}$. These manifolds interact with manifolds of the same J within excited terms. We account for this mixing in determining corrections to the Landé interval rule for the relative energy positions of the J manifolds within the ^4I term. However, our calculation of the crystal-field matrix elements within the ^4I term neglects any corrections to the ^4I wave functions resulting from spin-orbit mixing with higher-energy terms. This method and level of approximation are identical to those of Refs. 9–12.

The Nd^{3+} ion occupies a site of D_{2d} symmetry that completely lifts the degeneracy of each of the J manifolds, except for the twofold Kramers degeneracy. The structure for Y(Gd)VO is given by Wyckoff.[13] (See Fig. 9). The nearest neighbors to the Nd^{3+} ion are four O^{2-} ions (labeled A,B,C,D in Fig. 9) that form a tetragonally distorted tetrahedron. The next-nearest neighbors are also four O^{2-} ions that form a second tetragonally distorted tetrahedron, but these are sufficiently far away that we need consider only the effects of the nearest neighbors.

Traditionally, the crystal field is expanded in terms of operators C_{kq} transforming as the kqth spherical harmonic, cf. Ref. 12. This method uses parameters B_{kq} associated with these operators. The crystal-field Hamiltonian for an f electron at a site of D_{2d} symmetry is then

$$\mathcal{H}_{cf}=B_{20}C_{20}+B_{40}C_{40}+B_{60}C_{60}+B_{44}(C_{44}+C_{4-4})+B_{64}(C_{64}+C_{6-4})\ . \quad (1)$$

This expression facilitates the calculation of the crystal-field matrix elements, and before high-speed computers were readily available, this was the most important consideration. Unfortunately, such a description of the crystal field does not easily lend itself to a useful physical interpretation. So while the parameters B_{kq} appear often in the literature, they are rarely discussed or applied to other problems.

We present here a different approach towards the calculation of crystal-field parameters. We expand the field in terms of operators transforming as the irreducible representations of the tetrahedral group T_d. Since we are using a basis set that more closely represents the symmetry of the crystal field, the number of off-diagonal matrix elements is reduced. This leads to a definite advantage in interpreting the fitting parameters.

The f states span the irreducible representations a_1, t_1, and t_2 of the T_d group. The combinations of the $l=3$ spherical harmonics that make up the states of these representations are

$$\begin{aligned}
|a_1\rangle &= -\frac{i}{\sqrt{2}}|3,-2\rangle+\frac{i}{\sqrt{2}}|3,2\rangle \sim xyz\ ,\\
|t_{2\xi}\rangle &= \frac{\sqrt{5}}{4}|3,-3\rangle-\frac{\sqrt{3}}{4}|3,-1\rangle+\frac{\sqrt{3}}{4}|3,1\rangle\\
&\quad -\frac{\sqrt{5}}{4}|3,3\rangle \sim (5x^2-3r^2)x\ ,\\
|t_{2\eta}\rangle &= -\frac{i\sqrt{5}}{4}|3,-3\rangle-\frac{i\sqrt{3}}{4}|3,-1\rangle-\frac{i\sqrt{3}}{4}|3,1\rangle\\
&\quad -\frac{i\sqrt{5}}{4}|3,3\rangle \sim (5y^2-3r^2)y\ ,\\
|t_{2\zeta}\rangle &= |3,0\rangle \sim (5z^2-3r^2)z\ , \qquad (2)\\
|t_{1x}\rangle &= -\frac{\sqrt{3}}{4}|3,-3\rangle-\frac{\sqrt{5}}{4}|3,-1\rangle+\frac{\sqrt{5}}{4}|3,1\rangle\\
&\quad +\frac{\sqrt{3}}{4}|3,3\rangle \sim (y^2-z^2)x\ ,\\
|t_{1y}\rangle &= -\frac{i\sqrt{3}}{4}|3,-3\rangle+\frac{i\sqrt{5}}{4}|3,-1\rangle+\frac{i\sqrt{5}}{4}|3,1\rangle\\
&\quad -\frac{i\sqrt{3}}{4}|3,3\rangle \sim (z^2-x^2)y\ ,\\
|t_{1z}\rangle &= \frac{1}{\sqrt{2}}|3,-2\rangle+\frac{1}{\sqrt{2}}|3,2\rangle \sim (x^2-y^2)z\ .
\end{aligned}$$

Included here are the real-valued third-order polynomials that serve as basis functions for these representations. From these polynomials, we can determine the shapes of the various wave functions. The a_1 state has eight lobes along the [111] directions. The t_2 states, on the other hand, have large lobes along the coordinate axes, e.g., $t_{2\zeta}$ has its lobes along the z axis. Finally, the t_1 states have eight lobes like the a_1 state, but these lobes are located in the planes formed by the coordinate axes. For example, the t_{1z} state has four lobes in the xz plane and four lobes in the yz plane, and each of these lobes is tilted away from the xy plane by $\pm 35°$. Our work demonstrates how we can interpret the crystal-field parameters in terms of the shapes of the wave functions and simple point-ion models.

Within the basis set $\{a_1, t_{2\xi}, t_{2\eta}, t_{2\zeta}, t_{1x}, t_{1y}, t_{1z}\}$, the crystal-field Hamiltonian for a site of D_{2d} symmetry is given by

$$\mathcal{H}_{cf}=\begin{vmatrix} -3(\beta+\gamma) & 0 & 0 & 0 & 0 & 0 & 0 \\ 0 & \beta-\frac{B}{2} & 0 & 0 & -Y & 0 & 0 \\ 0 & 0 & \beta-\frac{B}{2} & 0 & 0 & Y & 0 \\ 0 & 0 & 0 & \beta+B & 0 & 0 & 0 \\ 0 & -Y & 0 & 0 & \gamma-\frac{C}{2} & 0 & 0 \\ 0 & 0 & Y & 0 & 0 & \gamma-\frac{C}{2} & 0 \\ 0 & 0 & 0 & 0 & 0 & 0 & \gamma+C \end{vmatrix} \tag{3}$$

The parameters β and γ give the splitting of the f states into a singlet a_1 and two triplets t_2 and t_1 by a tetrahedral field. The tetragonal distortion along the $z(c)$ axis, which results in the D_{2d} symmetry, splits each of the triplets into a doublet and a singlet, the $t_{2\zeta}$ and t_{1z} states being split off. This is described by the parameters B and C, respectively. Finally, the D_{2d} symmetry crystal field leads to a mixing between the $t_{2\xi}$ and t_{1x} states and between the $t_{2\eta}$ and t_{1y} states, as given by the parameter Y. A straightforward transformation can be used to convert these parameters into the parameters B_{kq} for comparison with previous results.

The crystal field is described in Eq. (3) in terms of one-electron cyrstal-field parameters. We then calculate, in terms of these parameters, the many-electron matrix elements of the crystal-field interaction between the states of the ^4I term. The positions of the various Stark levels are the result of simultaneously diagonalizing the spin-orbit and the crystal-field interactions.

TABLE II. Stark levels (cm^{-1}) of the ^4I J multiplets for Nd^{3+} in YVO_4.

J multiplet	Experimental	Calculated
$^4I_{9/2}$	0.0	0.0
	109.4	106.5
	174.9	169.9
	226.8	217.2
	439.0	444.0
$^4I_{11/2}$	1966.5	1966.9
	1987.5	1988.4
	2046.1	2046.8
	2061.5	2062.8
	2153.8	2159.1
	2181.0	2181.0
$^4I_{13/2}$	3909.6	3908.7
	3931.5	3934.1
	3978.6	3978.6
	4040.4	4046.3
	4087.7	4091.6
	4158.6	4161.0
	4167.4	4162.0
$^4I_{15/2}$	5833.1	5834.3
	5868.3	5872.6
	5915.4	5919.6
	6066.7	6061.0
		6168.3
	6260.6	6256.2
		6260.2
	6317.7	6317.7
$^4F_{3/2}$	11365.2	
	11383.5	

RESULTS AND DISCUSSION

We have performed a least-squares fit to the experimental levels given in Tables I and II. In addition to varying the five crystal-field parameters (β, γ, B, C, and Y), we also varied the energy positions of the $^4I_{11/2}$, $^4I_{13/2}$, and $^4I_{15/2}$ manifolds relative to the $^4I_{9/2}$ manifold, thereby accounting for departures from the Landé interval rule that arise from the mixing with excited state terms. Thus, we have eight independent parameters to fit more than 20 levels. The results of this fit are given in Tables III and IV for GVO and YVO, respectively. In each case, the root-mean-square deviation is less than 4 cm^{-1}, showing a very good fit to the experimental results. In order to compare with other calculations, we have also included our results expressed in terms of the B_{kq} parameters.

The first result from our fit is that the energy positions of the excited spin-orbit manifolds for the Nd^{3+} impurity in GVO are nearly identical to the energy positions in

TABLE III. Crystal-field parameters and J multiplet positions for the Nd^{3+} dopant in $GdVO_4$.

Crystal-field parameters (cm^{-1})		Energy levels (cm^{-1})
$\beta=178.2$	$B_{20}=-30.6$	
$\gamma=-50.8$	$B_{40}=578$	$E(^4I_{11/2})=1864$
$B=-332.5$	$B_{60}=-1077$	$E(^4I_{11/2})=3836$
$C=37.0$	$B_{44}=968$	$E(^4I_{15/2})=5877$
$Y=-118.7$	$B_{64}=-234$	

YVO. That these energy positions are similar results from the shielding f electrons by the closed $5s$ and $5p$ shells.

We now examine the crystal-field parameters. We note that the differences between the two sets is very slight. In general, the parameters for the GVO host are slightly smaller than those for the YVO host. This can be explained in a simple fashion by considering the dimensions of the host crystal. The lattice constants for GVO are larger than those for YVO,[13] leading to a weaker crystal-field in the case of GVO. Finally, we note that the parameters B_{kq} for Nd:YVO from our fit are in good agreement with those of Karayianis, Morrison, and Wortman.[12]

The signs of the crystal-field parameters (β, γ, B, C, Y) can be partially explained by considering the shapes of the wave functions and the positions of the neighbors as shown in Fig. 9. We note that the directions of the coordinate axes shown in this figure are somewhat atypical. Our choice of x and y axes are rotated by 45° from the usual choice in which the symmetry planes bisect the x and y axes. We have chosen the axis system in Fig. 9 since it leads to a very simple interpretation of the crystal-field parameters. In our coordinate system, the four O^{2-} ions are very nearly on the x and y axes. Therefore, the lobes of the $t_{2\xi}$ and $t_{2\eta}$ electron states are nearly directed towards the negatively charged O ions, making these the highest-energy states. In contrast to this is the a_1 state, whose lobes point along the [111] directions, away from the O^{2-} ions. Hence, the a_1 state is the most energetically favorable state. In between these extremes are the $t_{2\zeta}$ and t_1 states. The $t_{2\zeta}$ is expected to lie below the $t_{2\xi}$ and $t_{2\eta}$ states in energy because there are no O ions along the z axis as there are along the x and y axes. Within the t_1 states, the t_{1z} is expected to be the most energetic state since its lobes are directed more towards the O^{2-} ions than are the lobes of each of the states t_{1x} and t_{1y}. The splittings of the t_1 and t_2 manifolds are consistent with B being negative and C being positive. In addition, the signs and relative sizes of β and γ are also understood in terms of these ideas. As stated previously, the parameter Y mixes the states $t_{2\xi}$ and t_{1x} and the states $t_{2\eta}$ and t_{1y}. However, since the energy difference between the pairs of states $\{t_{2\xi},t_{2\eta}\}$ and $\{t_{1x},t_{1y}\}$ is large compared to Y, the actual mixing of the wave functions is only about 6%. The real effect of Y is to push these two pairs of states farther apart in energy. The amount of the energy shift of each pair of states to order Y^2 is given by

$$E_{\text{shift}}=\frac{Y^2}{(\beta-B/2)-(\gamma-C/2)} . \tag{4}$$

We see that our choice of representation for the f electrons does indeed lead to an explanation of the central elements of the crystal-field parameters in terms of a simple point-ion model.

TABLE IV. Crystal-field parameters and J multiplet positions for the Nd^{3+} dopant in YVO_4.

Crystal-field parameters (cm^{-1})		Energy levels (cm^{-1})
$\beta=190.6$	$B_{20}=-141$	
$\gamma=-59.7$	$B_{40}=616$	$E(^4I_{11/2})=1866$
$B=-386.0$	$B_{60}=-1158$	$E(^4I_{11/2})=3836$
$C=28.9$	$B_{44}=1008$	$E(^4I_{15/2})=5872$
$Y=-98.6$	$B_{64}=-285$	

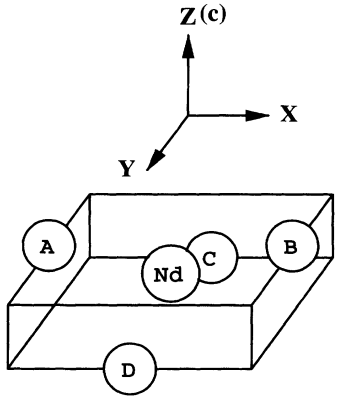

FIG. 9. The four O^{2-} neighbors surrounding the Nd dopant in Y(Gd)VO_4. These four O ions (A,B,C,D) form a tetragonally distorted tetrahedron with the distortion axis (z) corresponding to the c axis of the crystal.

We have presented here a detailed spectroscopic study and crystal-field analysis of Nd:GVO. For comparison, we have included a similar analysis of Nd:YVO. Our cyrstal-field parameters vary only slightly between these two systems, indicating that there are only slight differences in the crystal field at the Nd site between these two crystals. These differences can be explained in general terms by the larger lattice constants found in GVO compared to YVO. Our crystal-field analysis involved the expansion of the crystal field in terms of operators transforming as the irreducible representations of the T_d group. We see that this method leads to an easy and intuitive interpretation of the crystal-field parameters in terms of the shapes of the f wave functions and point-ion structural models. This interpretation may well help to explain other effects such as the response of the levels to pressure and the coupling of the dopant to various phonons, which will help to understand nonradiative decay, lattice relaxation, and phonon-assisted energy transfer. The increased understanding of the crystal-field parameters and the potential to help explain other important effects serves as justification for the employment of this method of crystal-field analysis.

ACKNOWLEDGMENTS

The authors want to thank B.H.T. Chai for his great generosity in supplying our samples.

[1]B. Chai, G. Loutts, X. X. Zhang, P. Hong, M. Bass, I. A. Shcherbakov, and A. I. Zagumennyi, *Advanced Solid-State Lasers* (Optical Society of America, Washington, D.C., 1994), pp. 230–232.

[2]V. G. Ostroumov, I. A. Shcherbakov, A. I. Zagumennyi, G. Huber, T. Jensen, and J. P. Meyn, in *OSA Proceedings of the Conference on Advanced Solid-State Lasers,* edited by A. A. Pinto and T. Y. Fan (Optical Society of America, Washington, D.C., 1993), pp. 64–67.

[3]Atomet, Inc., 222 Sherwood Avenue, Farmingdale, NY 11735-1718.

[4]F. G. Anderson, H. Weidner, P. L. Summers, R. E. Peale, X. X. Zhang, and B. H. T. Chai, J. Lumin. **60&61**, 150 (1994).

[5]F. G. Anderson, H. Weidner, P. L. Summers, R. E. Peale, and B. H. T. Chai, J. Lumin. (to be published).

[6]F. G. Anderson, H. Weidner, P. L. Summers, R. E. Peale, and B. H. T. Chai, in *New Materials for Advanced Solid State Lasers,* edited by B. H. T. Chai, T. Y. Fan, S. A. Payne, A. Cassanho, and T. H. Allik, MRS Symposia Proceedings No. 329 (Materials Research Society, Pittsburgh, 1994), p. 203.

[7]These crystals were grown by I. A. Scherbakov and A. I. Zagumennyi, General Physics Institute, Russian Academy of Sciences, Moscow, Russia.

[8]Kh.S. Bagdasarov, G. A. Bogomolova, A. A. Kaminskii, and V. I. Popov, Dokl. Akad. Nauk **SSSR 180,** 1347 (1968) [Sov. Phys. Dokl. **13,** 516 (1968)].

[9]N. Karayianis, J. Chem. Phys. **53,** 2460 (1970).

[10]N. Karayianis and R. T. Farrar, J. Chem. Phys. **53,** 3436 (1970).

[11]N. Karayianis, J. Phys. Chem. Solids **32,** 2385 (1971).

[12]N. Karayianis, C. A. Morrison, and D. E. Wortman, J. Chem. Phys. **62,** 4125 (1975).

[13]R. W. G. Wyckoff, *Crystal Structures,* 2nd ed. (Wiley, New York, 1965), Vol. 3, pp. 15–18.